RESEARCH NOTE

THE PROTEIN SOCIETY · WILEY

Dimerization of the CNNM extracellular domain

Ashkan Shahsavan [ID] | Emma L. Lee | Katalin Illes | Guennadi Kozlov | Kalle Gehring

Department of Biochemistry & Centre de recherche en biologie structurale, McGill University, Montreal, Canada

Correspondence
Kalle Gehring, Department of Biochemistry, McGill University, 3649 Prom. Sir-William-Osler, Montreal QC H3G 0B1, Canada.
Email: kalle.gehring@mcgill.ca

Abstract

Cystathionine-β-synthase (CBS)-pair domain divalent metal cation transport mediators (CNNMs) are an evolutionarily conserved family of magnesium transporters. They mediate magnesium homeostasis directly by transport of Mg^{2+} ions and indirectly by regulation of the transient receptor potential ion channel subfamily M member 7 (TRPM7). Here, we report the crystal structure of the extracellular domain of tapeworm CNNM4. The domain forms a dimer of immunoglobulin-like (Ig-like) folds with electron density observed for three glycosylation sites. Analytical ultracentrifugation confirms that mutations in the extracellular domain of human CNNM4 prevent its dimerization. An analogous mutation in mouse CNNM2 impairs its activity in a cellular assay of Mg^{2+} transport.

KEYWORDS

CNNM, crystal structure, extracellular domain, glycosylation, immunoglobulin-like, Jalili syndrome, magnesium, transporter

1 | INTRODUCTION

As the second most abundant cation in cells, magnesium is essential to the cellular function. It participates in a wide variety of biochemical processes, including binding to DNA and stabilizing its structure, serving as a cofactor in over 600 enzymatic reactions such as protein synthesis, DNA repair, and glycolysis, and contributing to cell signaling and proliferation (de Baaij et al., 2015).

Magnesium homeostasis in cells is regulated by various ion channels and transporters (Franken et al., 2022). Cystathionine-β-synthase (CBS)-pair domain divalent metal cation transport mediators (CNNMs) and their prokaryotic orthologues, CorB/C proteins, are a family of cation transporters implicated in magnesium homeostasis

(Wang et al., 2003). There are four CNNM isoforms in mammals, CNNM1 through CNNM4. CNNM2 and CNNM4 possess Mg^{2+} efflux activity facilitating renal/intestinal (re)absorption of magnesium ions (Stuiver et al., 2011; Yamazaki et al., 2013). Studies have revealed mutations in CNNM2 and CNNM4 of patients diagnosed with hypomagnesemia and Jalili syndrome, respectively (Parry et al., 2009; Polok et al., 2009; Stuiver et al., 2011). CNNM4 has also been implicated in sensitivity to non-alcoholic steatohepatitis and acetaminophen toxicity (Gonzalez-Recio et al., 2022; Simon et al., 2021). The interaction of CNNMs with PRL phosphatases impairs the CNNM transport function, resulting in elevated intracellular magnesium levels and promoting the progression of metastatic cancer (Funato et al., 2014; Hardy et al., 2015). Additionally, recent findings have demonstrated an interaction between CNNM proteins and

Reviewing Editor: John Kuriyan

another Mg^{2+} transporter, TRPM7 (Bai et al., 2021; Hardy et al., 2023; Kollewe et al., 2021; Mahbub et al., 2023).

Eukaryotic CNNMs possess four structural domains: an N-terminal extracellular domain (ECD), the pair of transmembrane and CBS-pair domains that are conserved in both prokaryotes and eukaryotes, and a C-terminal cyclic-nucleotide binding homology domain (CNBH) (Figure 1a) (Chen & Gehring, 2023; Gimenez-Mascarell et al., 2019). Crystal structures of the cytosolic CBS-pair and CNBH domains showed both domains form dimers and elucidated some of the regulatory roles of these domains (Chen et al., 2018; Chen et al., 2020; Corral-Rodriguez et al., 2014). While no structures are known for the eukaryotic transmembrane domains, domains from archaeal and bacterial orthologs have been crystallized (Chen et al., 2021; Huang et al., 2021). Those studies confirmed that domains function as dimers to mediate divalent cation (Mg^{2+}) transport across membranes. In contrast, little is known about the structure of the extracellular domains of CNNMs.

The extracellular domains of CNNM proteins play a major role in the proper localization of the proteins to the plasma membrane. The extracellular location on the surface of the plasma membrane was first demonstrated for the domain from CNNM2. The domain was further shown to be N-glycosylated at Asn-112 and the glycosylation was shown to be necessary for CNNM2 stability on the plasma membrane (de Baaij et al., 2012). Although the sequences of the extracellular domains are not highly conserved (Figure 1b), the domains are important for biological function of CNNM proteins and the site of disease causing mutations (Arjona et al., 2014).

Despite its importance for CNNM localization and stability, the structure of the extracellular domain has not been studied to date. Here, we present the crystal structure of the domain of CNNM4 from *Echinococcus granulosus* (*Eg*CNNM4) and demonstrate the domain has an immunoglobulin-like (Ig-like) fold with an extended dimerization interface. Additionally, we observed that *Eg*CNNM4 is glycosylated at Asn-51, Asn-63 and Asn-129 residues. Using mutagenesis and sedimentation velocity analytical ultracentrifugation (SV-AUC), we demonstrate that the extracellular domains of both human and *Eg*CNNM4 form dimers in solution and that the dimerization interface is required for proper function. The study provides a structural foundation for understanding CNNM regulation and function.

2 | RESULTS

2.1 | Structure of the CNNM4 extracellular domain

The extracellular domains from CNNM4 from four different species were expressed in *Sf*9 insect cells and subjected to crystallization screening. Crystals of the best
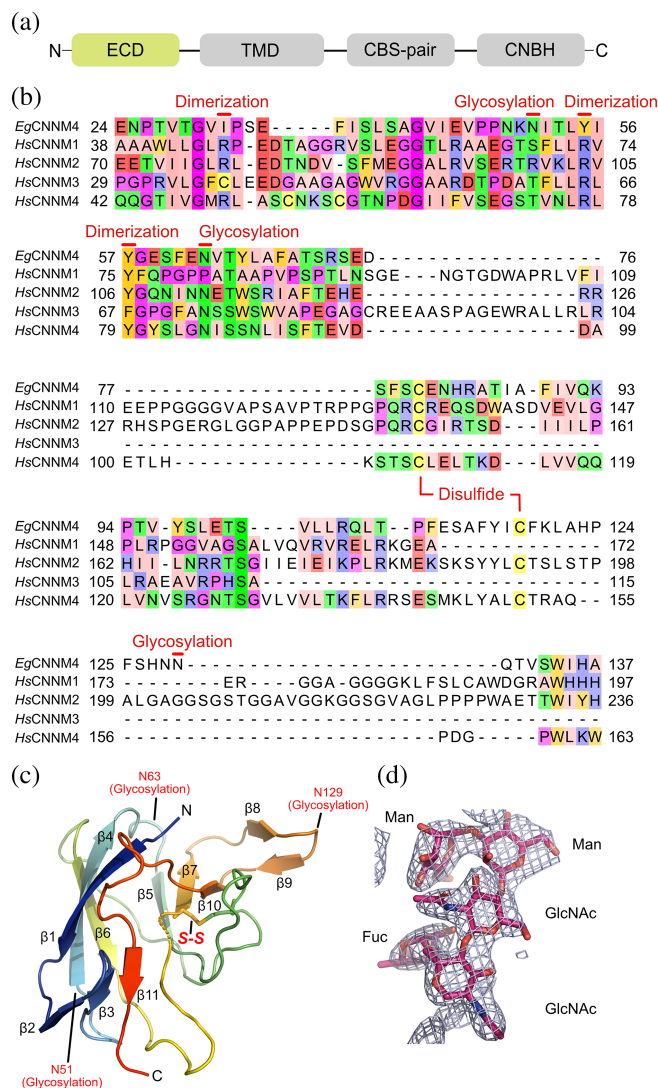

FIGURE 1 Immunoglobulin-like (Ig-like) fold of the *Eg*CNNM4 extracellular domain. (a) Domain organization of eukaryotic CNNMs: extracellular domain (ECD), transmembrane domain (TMD), CBS-pair domain, cyclic-nucleotide binding homology (CNBH) domain. (b) Sequence alignment of the extracellular domain of CNNM proteins. Residues involved in dimerization and sites of glycosylation are indicated. The listed CNNM orthologs and their UniProt accession numbers are as follows: *Eg*CNNM4 (*Echinococcus granulosus*; W6USS8), *Hs*CNNM1 (*Homo sapiens*; Q9NRU3), *Hs*CNNM2 (*Homo sapiens*; Q9H8M5), *Hs*CNNM3 (*Homo sapiens*; Q8NE01), *Hs*CNNM4 (*Homo sapiens*; Q6P4Q7). (c) Cartoon representation of *Eg*CNNM4 extracellular domain with the disulfide (S-S) and glycosylation sites (N51, N63, N129) labeled. D, $2F_o\text{-}F_c$ composite omit map of the glycan attached to Asn-51, contoured at 1.0 σ.

expressing construct, *Eg*CNNM4 (UniProt ID: W6USS8; residues 25–153), diffracted to 2.7 Å using synchrotron radiation and the structure solved by molecular replacement using an AlphaFold2 model (Mirdita et al., 2022) (Table 1). The asymmetric unit of the crystal contained eight molecules of the extracellular domain, which could

TABLE 1 Statistics of data collection and refinement.

PDB code	8GK6
Data collection	
X-ray source	CLS 08ID-1
Wavelength (Å)	0.9537
Space group	P 1 21 1
Cell dimensions	
a, b, c (Å)	55.34, 120.76, 95.25
α, β, γ (°)	90, 98.09, 90
Resolution (Å)	50–2.7 (2.72–2.7)[a]
R_{merge}	0.096 (0.727)
$I/\sigma I$	14 (1.2)
Completeness (%)	97.4 (86.6)
Redundancy	4.7 (3.0)
$CC_{1/2}$	0.99 (0.622)
Refinement	
Resolution (Å)	46.64–2.7
No. reflections	29,176
R_{work}/R_{free}	0.199/0.252
No. atoms	
Protein	8067
B-factor (Å^2)	
Protein	43.66
RMSDs	
Bond lengths (Å)	0.006
Bond angles (°)	1.83
Ramachandran statistics (%)	
Most favored regions	95.36
Additional allowed regions	4.45
Disallowed regions	0.2

[a]Highest resolution shell is shown in parentheses.

be superposed with an average root mean square deviation (RMSD) of 0.3 Å (Supp. Figure S1).

The structure of the *Eg*CNNM4 extracellular domain belongs to the immunoglobulin-like (Ig-like) fold found in diverse proteins (Figure 1c). Ig-like domains share a similar folding pattern characterized by a β-sandwich, formed by two facing β-sheets containing antiparallel strands. They have various functions such as cell adhesion, protein–protein interaction, receptor-ligand recognition, enzyme activity, and immune system regulation (Barclay, 2003; Bork et al., 1994). The *Eg*CNNM4 extracellular domain consists of 11 β strands forming a β-sandwich (Figure 1c). A disulfide bond between conserved cysteines, Cys-80 and Cys-118, connects strand β7 and the loop between strands β4 and β5.

2.2 | N-glycosylation of CNNM extracellular domain

The extracellular domain of *Eg*CNNM4 possesses three asparagine residues in N-X-S/T motifs: Asn-51, Asn-63, and Asn-129. Asn-63 is conserved in *Eg*CNNM4 and all human CNNMs except CNNM1 (Figure 1b). In the crystal structure, we observed well-defined glycan electron densities at all 3 N-glycosylation sites (Figures 1d and S1). The mature N-glycan product in insect cells is Man$_3$-GlcNAc($\pm\alpha$3/6Fuc)GlcNAc (Shi & Jarvis, 2007).

2.3 | CNNM4 extracellular domain dimerization

As CNNMs are dimers, we examined the crystal packing of the *Eg*CNNM4 extracellular domain for potential dimerization interfaces. Ig-like domains often form homodimers or heterodimers with Ig-like domains of other proteins (Barclay, 2003; Bork et al., 1994). Two types of interdomain contacts were observed: one via loops and the other via β-strands containing hydrophobic residues (Figure 2a). We hypothesized the latter surface represents the biologically relevant dimerization interface. This was supported by the PISA analysis (Krissinel & Henrick, 2007) which predicted the second interface was more stable. For experimental verification, we turned to sedimentation velocity analytical ultracentrifugation (SV-AUC) to measure the oligomerization state in solution. Analysis of the wild-type domain identified a single species with sedimentation coefficient (S) of 2.79, corresponding to a molecular weight of 35.4 kDa (Figure 2b), almost exactly twice the theoretical molecular weight of the construct (15.5 kDa) with three glycans.

To confirm identification of the dimerization surface, we generated two mutants, I32R and Y57A, targeting residues within the second interface. After purification, both mutants tended to aggregate with a large peak eluting in the void volume in size-exclusion chromatography (Supp. Figure S2). SV-AUC analysis of the mutants showed broad peaks at higher sedimentation coefficient confirming that the mutations disrupted the dimerization of the domain (Figure 2b). Exposure of the hydrophobic interactions within the dimerization surface is likely responsible for the aggregation and the broad sedimentation peak of the mutants.

To study the dimerization of the extracellular domain in humans, we generated a dimeric model of human CNNM4 (*Hs*CNNM4; UniProt ID: Q6P4Q7) using AlphaFold-multimer (Evans et al., 2021). The dimerization mode in the predicted model of *Hs*CNNM4 extracellular domain is similar to that of the *Eg*CNNM4 crystal
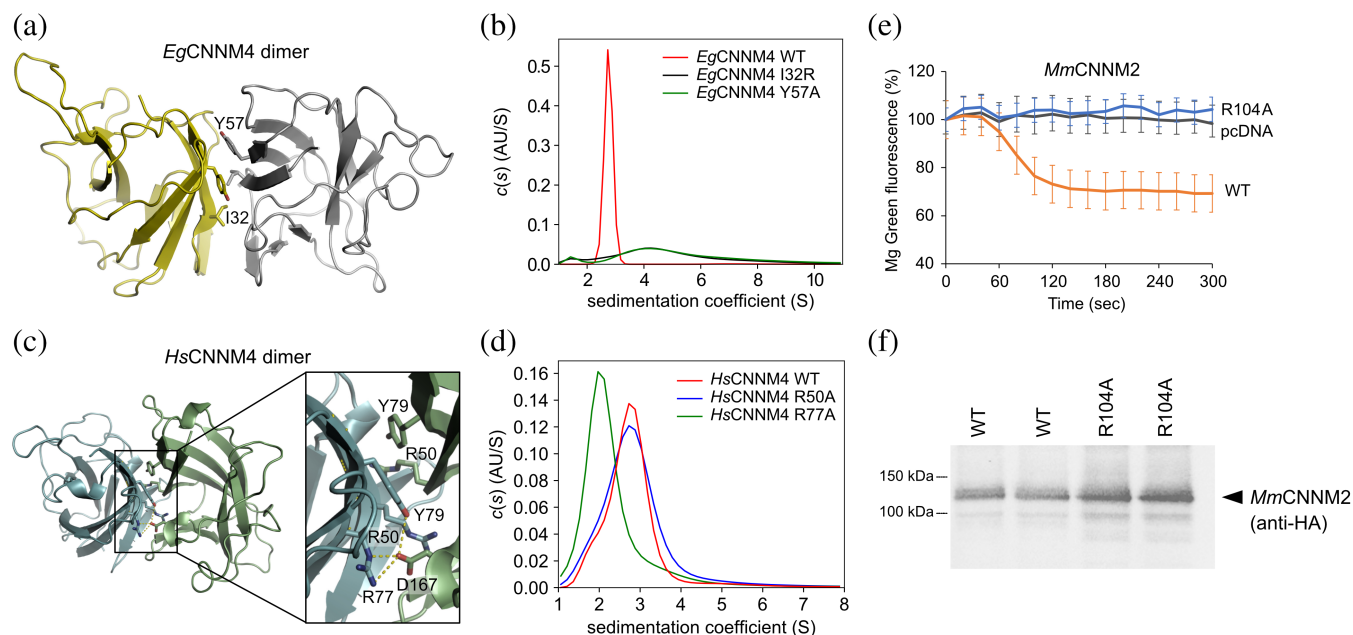
FIGURE 2 Mutagenesis of the extracellular domain disrupts dimerization and Mg^{2+} transport. (a) Structure of the dimer of *Eg*CNNM4 extracellular domain. (b) Sedimentation velocity analytical ultracentrifugation (SV-AUC) experiments with wild-type (WT) and mutant *Eg*CNNM4 (25–153). (c) Model of the dimer of the *Hs*CNNM4 extracellular domain predicted by AlphaFold-multimer. (d) SV-AUC experiments with *Hs*CNNM4 (44–175). (e) Mg^{2+} efflux assays in HEK293T cells transfected with WT or R104A mouse CNNM2 or negative control (pcDNA). R104A in *Mm*CNNM2 corresponds to R77A in *Hs*CNNM4. *p*-value = 0.00827 comparing the WT and R104A mutant was calculated using a two-tailed Student t-test. Each measurement represents the average of three independent transfections. For each transfection, the average of 10 cells are measured. The bars are relative standard errors (RSE). F, Western blotting analysis of HEK293T cells transfected with HA-tagged *Mm*CNMM2 mCherry WT and HA-tagged *Mm*CNNM2 mCherry-HA R104A shows slighlty higher expression of the R104A mutant than the wild-type *Mm*CNNM2-mCherry fusion proteins. Two replicates of each transfection are shown. WT, wild-type.

structure (Figure 2a,c). Surprisingly, several residues in hydrophobic interface are replaced by arginine residues, Arg-50 and Arg-77 (Figure 2c). Arg-50 in *Hs*CNNM4 corresponds to Ile-32 in *Eg*CNNM4, Arg-77 is conserved among all members of human CNNM and Tyr-79 is conserved between *Eg*CNNM4 and human CNNMs (Figure 1b). We carried out SV-AUC analysis to confirm that *Hs*CNNM4 (residues 44–175) dimerizes. Using the same analysis as before, a peak was observed at sedimentation coefficient (S) of 2.99, corresponding to a molecular weight of 36.7 kDa, demonstrating the domain exists as a dimer (Figure 2d).

We used mutagenesis to identify the dimerization interface. *Hs*CNNM4 R50A and R77A mutants were generated, and AUC analysis performed. While *Hs*CNNM4-R50A sedimented as a dimer (like the wild-type protein), a peak at sedimentation coefficient (S) of 2.01 was observed for *Hs*CNNM4-R77A, corresponding to a molecular weight of 18.1 kDa, as expected for a monomer (Figure 2d). Therefore, Arg-77 is essential to the dimerization of *Hs*CNNM4 extracellular domain in solution. A third mutant, Y79A, was generated but size-exclusion chromatography indicated aggregation (Supp. Figure S2) so it was not analyzed by SV-AUC. According to the structural model, Arg-77 and Tyr-79

interact with Asp-167 (Figure 2d), a residue that is conserved in human CNNM2 (UniProt ID: Q9H8M5) and CNNM4 (Figure 1b). We also studied four *Hs*CNNM4 mutations in the extracellular domain associated with Jalili syndrome. All the mutants (N85D, E95Q, M145T and A149S) sedimented as dimers in the SV-AUC experiments (Supp. Figure S2).

2.4 | The effect of the extracellular domain dimerization on Mg^{2+} efflux

Mg^{2+} transport activity of CNNMs can be measured in cells using a fluorescent indicator, Magnesium Green, that measures cytosolic Mg^{2+} levels (Yamazaki et al., 2013). We implemented this assay to test whether disruption of the extracellular domain dimerization affects CNNM transport activity (Figure 2e). HEK-293T cells were transfected with either an HA-tagged mouse CNNM2 (UniProt ID: Q3TWN3) mCherry fusion protein or HA-tagged mouse CNNM2 R104A mCherry fusion mutant. Arg-104 in mouse CNNM2 corresponds to Arg-77 in human CNNM4 that plays a key role in dimerization of *Hs*CNNM4 extracellular domain (Figure 2c). Cells

expressing wild-type CNNM2 showed a 30% drop in fluorescent levels, while cells transfected with an empty vector showed little or no drop. Cells expressing CNNM2 R104A mutant showed no efflux (Figure 2e) despite an expression level even slightly higher than that of the wild-type protein (Figures 2f and S4). Thus, disruption of dimerization of the extracellular domain impairs CNNM Mg^{2+} efflux activity.

3 | DISCUSSION

Ig-like domains are present in diverse proteins and commonly found as extracellular domains of membrane proteins. The Ig-like fold can be categorized into two main topologies: c-type (constant) with seven β strands and v-type (variable) with nine β strands. Within these, other types exist such as s-type (switched) with seven strands, where the fourth strand has switched sheets, and h-type (hybrid) with eight strands (Bork et al., 1994). The crystal structure of EgCNNM4 extracellular domain deviates from the aforementioned as it contains 11 β strands with a different arrangement between the sheets. While a disulfide bond is a frequent characteristic of Ig-like domains, it is not necessary for the structure and Ig-like-domains lacking the disulfide bond are known (Barclay, 2003; Bork et al., 1994). Among four human CNNMs, CNNM3 has the smallest extracellular domain and lacks one of the cysteines for a disulfide bond. DALI (Holm et al., 2023) and Foldseek (van Kempen et al., 2023) searches using the structure of EgCNNM4 extracellular domain revealed the IPT/TIG domains of early B-cell factor 1 (EBF1) and Plexin-C1 as the best hits. Despite the low 13% sequence identity, the EBF1 structure (pdb: 3MQI) can be superposed on the structure of EgCNNM4 extracellular domain with a root mean square deviation (RMSD) of 1.1 Å. IPT/TIG domains (Pfam: PF01833) have an Ig-like fold and are found in transcription factors and cell surface receptors such as MET, VESPR and Plexins (Bork et al., 1999). It is noteworthy that the IPT/TIG domains in both EBF1 and EBF3 form dimers through their β-strands similarly to dimerization of CNNM extracellular domains (Siponen et al., 2010). The dimerization mode through β-strands is similar between HsCNNM4 and EgCNNM4 extracellular domains. Curiously, while the dimerization interface of EgCNNM4 predominantly involves hydrophobic interactions, the dimerization interface of HsCNNM4 is characterized by electrostatic interactions between arginine and aspartate residues.

Proper folding and dimerization of the extracellular domain appears to be required for CNNM function. The loss of human CNNM2 Mg^{2+} efflux activity when the dimerization interface was mutated could reflect a regulatory role of the N-terminal domain or improper localization of the mutant protein. Other N-terminal domain mutations have been associated with reduced cell surface expression. Asn-112, a glycosylation site in HsCNNM2 (equivalent to Asn-85 in HsCNNM4), is required for the correct CNNM2 membrane localization (de Baaij et al., 2012). Modification of N-glycosylation of the extracellular domain has been suggested as the mechanism for CNNM regulation by ADP-ribosylation factor-like protein 15 (ARL15) (Zolotarov et al., 2021). Similarly, the E122K mutation in HsCNNM2 (Figure 1b) has been associated with reduced cell surface expression (Arjona et al., 2014). None of the HsCNNM4 extracellular domain mutants that are associated with Jalili syndrome disrupted dimerization of this domain in AUC experiments (Supp. Figure S2). This implies that the mutations leading to the disease are likely attributable to other factors. Along with dimerization, proper folding and glycosylation of CNNM extracellular domains likely play a large role in protein localization in polarized cells in tissues (Vagin et al., 2009).

4 | MATERIALS AND METHODS

4.1 | Expression and purification of recombinant proteins

The extracellular domains of CNNM4 from human (UniProt ID: Q6P4Q7; residues 44–175), tapeworm Echinococcus granulosus (UniProt ID: W6USS8; residues 25–153), tardigrade (UniProt ID: A0A1D1VJA9; residues 44–164) and fruit fly Drosophila melanogaster (UniProt ID: A0A0B7P9G0; residues 55–182) were produced in Sf9 insect cells as fusion proteins with an N-terminal melittin signal peptide MKFLVNVALVFMVVYISYIYA which is cleaved co-translationally, followed by a hexahistidine tag DRHHHHHHGS which remains as part of the purified proteins. Expression under control of a polyhedrin promoter was carried out at 27°C for 68 h in I-Max medium (Wisent). The secreted proteins were purified from the culture media by immobilized metal affinity chromatography (IMAC) Ni-NTA resin (QIAGEN), washed with buffer (25 mM Tris–HCl pH 7.5, 500 mM NaCl, 10 mM imidazole) and eluted with the same buffer containing 250 mM imidazole. The affinity-purified protein was further purified by size exclusion chromatography on a Superdex 200 10/300 GL (GE Healthcare) in HPLC buffer (10 mM Tris–HCl pH 7.5, 100 mM NaCl) (Supp. Figure S2).

4.2 | Crystallization

Crystals of *Eg*CNNM4 construct were obtained using sitting drop vapor diffusion technique with the Classics II screen (QIAGEN). The final concentration of the protein in the drop was 2.5 mg/mL. The best crystal was obtained from condition containing 0.1 M Tris pH 8.5, 25% (w/v) PEG6000. For data collection, crystals were cryoprotected by soaking in the reservoir solution supplemented with 30% (v/v) ethylene glycol.

4.3 | Structure solution and refinement

Diffraction data from the crystal of *Eg*CNNM4 (residues 25–153) were collected at the Canadian Light Source (CLS). Data processing and scaling were performed using HKL-2000 (Otwinowski & Minor, 1997). The initial phases were determined by molecular replacement with Phaser (McCoy et al., 2007), using an AlphaFold2 model of *Eg*CNNM4 (Mirdita et al., 2022). The initial phases were improved by Autobuilder in PHENIX package (Adams et al., 2010). The starting protein model was then completed and adjusted with the program Coot (Emsley & Cowtan, 2004) and improved by multiple cycles of refinement, using the program phenix.refine (Adams et al., 2010) and model refitting. None of the nonnative residues are visible in the crystal structure. All residues of *Eg*CNNM4 (residues 25–153) are visible in the crystal structure except the last residue (T153) which is only visible in some copies of the asymmetric unit of the crystal. The coordinates have been deposited on the Protein Data Bank (PDB) under the accession number 8GK6.

4.4 | Sedimentation-velocity analytical ultracentrifugation (SV-AUC)

Sedimentation velocity AUC experiments were performed at 20°C using a Beckman Coulter XL-I analytical ultracentrifuge using an An-60Ti rotor at 158,000g (45,000 rpm) for 18 h with scans performed every 60 s. A double-sector cell, equipped with a 12-mm Epon centerpiece and sapphire windows, was loaded with 380 and 400 μL of sample and buffer (10 mM Tris pH 7.5, 100 mM NaCl), respectively. 10 μM (0.15 mg/mL) each of *Hs*CNNM4 and *Eg*CNNM4 were monitored with UV at 280 nm. The data was analyzed with SEDFIT version 1501b using a continuous c(s) distribution (Schuck, 2000). Numerical values for the solvent density and viscosity were calculated to be 1.0026 g/cm^3 and 0.01014 mPa·s, respectively, using SEDNTERP. Partial specific volumes were defaulted to 0.73 cm^3/g, and the frictional ratio (f/f_0) values were floated. Residual and c(s) distribution graphs were plotted using GUSSI (Supp. Figure S3).

4.5 | Magnesium Green Mg^{2+} efflux assay

HEK-293 T cells were grown in poly-lysine coated 3.5 cm glass bottom plates and transfected with HA-tagged *Mm*CNNM2 mCherry fusion proteins (both wild type and mutant). Transfections were performed using lipofectamine 3000 when the cells were between 20% and 30% confluency, to ensure adequate separation for single cell analysis. Cells were grown in DMEM supplemented with 40 mM MgCl$_2$ for 24 h. Subsequently, cells were incubated in 800 μL Mg^{2+} loading buffer (78.1 mM NaCl, 5.4 mM KCl, 1.8 mM CaCl$_2$, 40 mM MgCl$_2$, 5.5 mM glucose, 5.5 mM HEPES, pH to 7.4 with KOH), with 2 mM Magnesium Green dye (Fisher Scientific) for 30 min in a 37°C CO$_2$ incubator. Cells were then rinsed with Mg^{2+} loading buffer at room temperature and observed via microscopy (AxioObserver.Z1 with X-cite series 120Q Illuminator, AxioCamMR3 camera, under the control of Axiovision software). Magnesium Green fluorescence (excitation 450–488 nm and emission 500–548 nm) was measured for 5 min (filter set ET-GFP 49002, objective ET Plan-Neofluar 10×/0.20 Ph 1) with 20 s between frames. At 1 min, the buffer was changed to Mg^{2+}-free buffer (138.1 mM NaCl, 5.4 mM KCl, 1.8 mM CaCl$_2$, 5.5 mM glucose, 5.5 mM HEPES, pH to 7.4 with KOH). Following the efflux assay, *Mm*CNNM2-mCherry expression was detected by measuring fluorescence from the ET-mCherry Texas Red 49008 filter set (excitation 540–580 nm and emission 590–670 nm). Magnesium Green fluorescence in cells expressing *Mm*CNNM2 was quantified in FIJI analysis software, and the average of 10 cells plotted as a function of time.

4.6 | Western blotting

HEK293T cells were grown in DMEM and transfected with HA-tagged *Mm*CNNM2 mCherry fusion proteins as described in the Mg Efflux assay. Cells were harvested 24 h post transfection. Cells were washed twice with PBS, and harvested in 1 mL PBS. Lysis was carried out with 0.5% Triton X-100 in PBS with protease inhibitors for 30 min on ice. Protein concentration was measured via Pierce BCA assay (Thermofisher). 10 μg of lysate sample was resolved via standard SDS-PAGE and western blot protocols. The Cell Signaling anti-HA (6E2) antibody (2367S) and secondary HRP conjugated anti mouse

(Jackson ImmunoResearch, 115-035-071) was used to detect the presence of *Mm*CNNM2-mCherry-HA. Biolegends anti-GAPDH (631402) and Jackson ImmunoResearch (111-035-046) were used to detect GAPDH to monitor lysate loading.

AUTHOR CONTRIBUTIONS

Ashkan Shahsavan: Investigation; writing – original draft; writing – review and editing. **Emma L. Lee:** Investigation. **Katalin Illes:** Investigation. **Guennadi Kozlov:** Investigation. **Kalle B. Gehring:** Supervision; writing – review and editing.

ACKNOWLEDGMENTS

CONFLICT OF INTEREST STATEMENT

The authors declare no conflicts of interest.

ORCID

Ashkan Shahsavan https://orcid.org/0009-0002-6465-9560

REFERENCES

Adams PD, Afonine PV, Bunkoczi G, Chen VB, Davis IW, Echols N, et al. PHENIX: a comprehensive python-based system for macromolecular structure solution. Acta Crystallogr D Biol Crystallogr. 2010;66(Pt 2):213–21.

Arjona FJ, de Baaij JH, Schlingmann KP, Lameris AL, van Wijk E, Flik G, et al. CNNM2 mutations cause impaired brain development and seizures in patients with hypomagnesemia. PLoS Genet. 2014;10(4):e1004267.

Bai Z, Feng J, Franken GAC, Al'Saadi N, Cai N, Yu AS, et al. CNNM proteins selectively bind to the TRPM7 channel to stimulate divalent cation entry into cells. PLoS Biol. 2021;19(12):e3001496.

Barclay AN. Membrane proteins with immunoglobulin-like domains–a master superfamily of interaction molecules. Semin Immunol. 2003;15(4):215–23.

Bork P, Doerks T, Springer TA, Snel B. Domains in plexins: links to integrins and transcription factors. Trends Biochem Sci. 1999;24(7):261–3.

Bork P, Holm L, Sander C. The immunoglobulin fold. Structural classification, sequence patterns and common core. J Mol Biol. 1994;242(4):309–20.

Chen YS, Gehring K. New insights into the structure and function of CNNM proteins. FEBS J. 2023;290:5475–95.

Chen YS, Kozlov G, Fakih R, Funato Y, Miki H, Gehring K. The cyclic nucleotide-binding homology domain of the integral membrane protein CNNM mediates dimerization and is required for Mg^{2+} efflux activity. J Biol Chem. 2018;293(52):19998–20007.

Chen YS, Kozlov G, Fakih R, Yang M, Zhang Z, Kovrigin EL, et al. Mg^{2+}-ATP sensing in CNNM, a putative magnesium transporter. Structure. 2020;28(3):324–335 e4.

Chen YS, Kozlov G, Moeller BE, Rohaim A, Fakih R, Roux B, et al. Crystal structure of an archaeal CorB magnesium transporter. Nat Commun. 2021;12(1):4028.

Corral-Rodriguez MA, Stuiver M, Abascal-Palacios G, Diercks T, Oyenarte I, Ereno-Orbea J, et al. Nucleotide binding triggers a conformational change of the CBS module of the magnesium transporter CNNM2 from a twisted towards a flat structure. Biochem J. 2014;464(1):23–34.

de Baaij JH, Hoenderop JG, Bindels RJ. Magnesium in man: implications for health and disease. Physiol Rev. 2015;95(1):1–46.

de Baaij JH, Stuiver M, Meij IC, Lainez S, Kopplin K, Venselaar H, et al. Membrane topology and intracellular processing of cyclin M2 (CNNM2). J Biol Chem. 2012;287(17):13644–55.

Emsley P, Cowtan K. Coot: model-building tools for molecular graphics. Acta Crystallogr D Biol Crystallogr. 2004;60(Pt 12 Pt 1:2126–32.

Evans R, O'Neill M, Pritzel A, Antropova N, Senior A, Green T, et al. Protein complex prediction with AlphaFold-multimer. bioRxiv. 2021;2021.10.04.463034.

Franken GAC, Huynen MA, Martinez-Cruz LA, Bindels RJM, de Baaij JHF. Structural and functional comparison of magnesium transporters throughout evolution. Cell Mol Life Sci. 2022;79(8):418.

Funato Y, Yamazaki D, Mizukami S, Du L, Kikuchi K, Miki H. Membrane protein CNNM4-dependent Mg^{2+} efflux suppresses tumor progression. J Clin Invest. 2014;124(12):5398–410.

Gimenez-Mascarell P, Gonzalez-Recio I, Fernandez-Rodriguez C, Oyenarte I, Muller D, Martinez-Chantar ML, et al. Current structural knowledge on the CNNM family of magnesium transport mediators. Int J Mol Sci. 2019;20(5):1135.

Gonzalez-Recio I, Simon J, Goikoetxea-Usandizaga N, Serrano-Macia M, Mercado-Gomez M, Rodriguez-Agudo R, et al. Restoring cellular magnesium balance through cyclin M4 protects against acetaminophen-induced liver damage. Nat Commun. 2022;13(1):6816.

Hardy S, Uetani N, Wong N, Kostantin E, Labbe DP, Begin LR, et al. The protein tyrosine phosphatase PRL-2 interacts with the magnesium transporter CNNM3 to promote oncogenesis. Oncogene. 2015;34(8):986–95.

Hardy S, Zolotarov Y, Coleman J, Roitman S, Khursheed H, Aubry I, et al. Prl-1/2 phosphatases control trpm7 magnesium-dependent function to regulate cellular bioenergetics. Proc Natl Acad Sci U S A. 2023;120(14):e2221083120.

Holm L, Laiho A, Toronen P, Salgado M. DALI shines a light on remote homologs: one hundred discoveries. Protein Sci. 2023;32(1):e4519.

Huang Y, Jin F, Funato Y, Xu Z, Zhu W, Wang J, et al. Structural basis for the Mg^{2+} recognition and regulation of the CorC Mg^{2+} transporter. Sci Adv. 2021;7(7):eabe6140.

Kollewe A, Chubanov V, Tseung FT, Correia L, Schmidt E, Rossig A, et al. The molecular appearance of native TRPM7 channel complexes identified by high-resolution proteomics. Elife. 2021;10:e68544.

Krissinel E, Henrick K. Inference of macromolecular assemblies from crystalline state. J Mol Biol. 2007;372(3):774–97.

Mahbub L, Kozlov G, Zong P, Lee EL, Tetteh S, Nethramangalath T, et al. Structural insights into regulation of CNNM-TRPM7 divalent cation uptake by the small GTPase ARL15. Elife. 2023;12:e86129.

McCoy AJ, Grosse-Kunstleve RW, Adams PD, Winn MD, Storoni LC, Read RJ. Phaser crystallographic software. J Appl Crystallogr. 2007;40(Pt 4):658–74.

Mirdita M, Schutze K, Moriwaki Y, Heo L, Ovchinnikov S, Steinegger M. ColabFold: making protein folding accessible to all. Nat Methods. 2022;19(6):679–82.

Otwinowski Z, Minor W. Processing of X-ray diffraction data collected in oscillation mode. Methods Enzymol. 1997;276:307–26.

Parry DA, Mighell AJ, El-Sayed W, Shore RC, Jalili IK, Dollfus H, et al. Mutations in CNNM4 cause Jalili syndrome, consisting of autosomal-recessive cone-rod dystrophy and amelogenesis imperfecta. Am J Hum Genet. 2009;84(2):266–73.

Polok B, Escher P, Ambresin A, Chouery E, Bolay S, Meunier I, et al. Mutations in CNNM4 cause recessive cone-rod dystrophy with amelogenesis imperfecta. Am J Hum Genet. 2009;84(2):259–65.

Schuck P. Size-distribution analysis of macromolecules by sedimentation velocity ultracentrifugation and Lamm equation modeling. Biophys J. 2000;78(3):1606–19.

Shi X, Jarvis DL. Protein N-glycosylation in the baculovirus-insect cell system. Curr Drug Targets. 2007;8(10):1116–25.

Simon J, Goikoetxea-Usandizaga N, Serrano-Macia M, Fernandez-Ramos D, Saenz de Urturi D, Gruskos JJ, et al. Magnesium accumulation upon cyclin M4 silencing activates microsomal triglyceride transfer protein improving NASH. J Hepatol. 2021;75(1):34–45.

Siponen MI, Wisniewska M, Lehtio L, Johansson I, Svensson L, Raszewski G, et al. Structural determination of functional domains in early B-cell factor (EBF) family of transcription factors reveals similarities to rel DNA-binding proteins and a novel dimerization motif. J Biol Chem. 2010;285(34):25875–9.

Stuiver M, Lainez S, Will C, Terryn S, Gunzel D, Debaix H, et al. CNNM2, encoding a basolateral protein required for renal Mg^{2+} handling, is mutated in dominant hypomagnesemia. Am J Hum Genet. 2011;88(3):333–43.

Vagin O, Kraut JA, Sachs G. Role of N-glycosylation in trafficking of apical membrane proteins in epithelia. Am J Physiol Renal Physiol. 2009;296(3):F459–69.

van Kempen M, Kim SS, Tumescheit C, Mirdita M, Lee J, Gilchrist CLM, et al. Fast and accurate protein structure search with foldseek. Nat Biotechnol. 2023. https://doi.org/10.1038/s41587-023-01773-0

Wang CY, Shi JD, Yang P, Kumar PG, Li QZ, Run QG, et al. Molecular cloning and characterization of a novel gene family of four ancient conserved domain proteins (ACDP). Gene. 2003;306:37–44.

Yamazaki D, Funato Y, Miura J, Sato S, Toyosawa S, Furutani K, et al. Basolateral Mg^{2+} extrusion via CNNM4 mediates transcellular Mg^{2+} transport across epithelia: a mouse model. PLoS Genet. 2013;9(12):e1003983.

Zolotarov Y, Ma C, Gonzalez-Recio I, Hardy S, Franken GAC, Uetani N, et al. ARL15 modulates magnesium homeostasis through N-glycosylation of CNNMs. Cell Mol Life Sci. 2021;78(13):5427–45.

SUPPORTING INFORMATION

Additional supporting information can be found online in the Supporting Information section at the end of this article.